Available online at www.sciencedirect.com
SCIENCE DIRECT®
Journal of Solid State Chemistry 177 (2004) 1695–1703
JOURNAL OF SOLID STATE CHEMISTRY
http://elsevier.com/locate/jssc

The structural and electric properties of the perovskite system $BaTiO_3$–$Ba(Fe_{1/2}Ta_{1/2})O_3$

Guobao Li,[a,*] Shixiang Liu,[a] Fuhui Liao,[a] Shujian Tian,[a] Xiping Jing,[a] Jianhua Lin,[a] Yoshiaki Uesu,[b] Kay Kohn,[b] K. Saitoh,[c] Masami Terauchi,[c] Naili Di,[d] and Zhaohua Cheng[d]

[a] *State Key Laboratory of Rare Earth Materials Chemistry and Applications, College of Chemistry and Molecular Engineering, Peking University, Chenfu Road 202, Beijing 100871, People's Republic of China*

[b] *Department of Physics, Waseda University, 3-4-1 Okubo, Shinjuku-ku, Tokyo 169-8555, Japan*

[c] *Division of Materials Analysis, Institute of Multidisciplinary Research for Advanced Materials, Tohoku University, 2-1-1 Katahira, Aoba-ku, Sendai 980-8577, Japan*

[d] *State Key Laboratory of Magnetism, Chinese Academy of Science, P.O. Box 603, Beijing 100080, People's Republic of China*

Received 29 October 2003; received in revised form 15 December 2003; accepted 18 December 2003

Abstract

Compounds in the pseudo-binary $BaTiO_3$–$Ba(Fe_{1/2}Ta_{1/2})O_3$ system have been synthesized at 1500°C in air and characterized by X-ray and electron diffraction as well as impedance analysis and Mössbauer spectroscopy. The symmetry of $Ba(Fe_{1/2}Ta_{1/2})O_3$ is found to be trigonal with the space group $P3m1$. Two solid solutions exist in the $BaTi_{1-x}Fe_{x/1}Ta_{x/1}O_3$ system at room temperature. The first (SS1) is in the composition range $0 \leqslant x \leqslant 0.07$ and is tetragonal, $P4mm$, while the second broader solid solution, (SS2) $0.12 \leqslant x \leqslant 1$, is trigonal and has the space group $P3m1$. The conductivity becomes higher with reduced amount of Ti in the structure. The activation energy of conductivity differs between the two solid solutions, 0.80 eV for SS1 and 0.30 eV for SS2, which indicates different mechanisms. The maximum of the real part of the permittivity recorded for compounds in SS1 decreases towards room temperature with increasing amount of Fe/Ta doping and a high dielectric constant of around 7000 is found for $BaTi_{0.94}Fe_{0.03}Ta_{0.03}O_3$.

Keywords: Relaxor; Structure; Space group P3*m*1; Perovskite; Conductivity and dielectric property; Barium iron tantalum oxide

1. Introduction

Relaxor ferroelectrics are characterized by their broad dielectric transition, known as the diffused phase transition with strong frequency dispersion. They have been the subjects of intense interests because they could be promising materials for use in non-volatile memory devices [1]. Up to now, the relaxor ferroelectric behavior occurs mainly in the lead-based materials [2–4]. In order to develop environment-friendly materials, considerable studies have been focused on the lead-free materials [5–29]. It is well known that $BaTiO_3$ has a paraelectric-to-ferroelectric transition at about 120°C with a very high dielectric constant. Thus, considerable attentions were paid to the doped $BaTiO_3$ [5–13] to modify the performance of the materials. However, the relaxor behavior of the doped $BaTiO_3$ was reported to occur at temperatures far above or below room temperature.

Recently, our research focused on systematic substitution of the *A*- and *B*-sites in the $BaTiO_3$-based materials aimed to obtain lead-free relaxor materials [30,31]. In this paper, we report the preparation of a pseudo-binary perovskite system $BaTiO_3-Ba(Fe_{1/2}Ta_{1/2})O_3$ and its structural and electric properties. Both $BaTiO_3$ and $Ba(Fe_{1/2}Ta_{1/2})O_3$ are described as typical perovskite-type compounds and could be expected to form a solid solution.

2. Experimental

The starting materials were analytical reagent grade $BaCO_3$, Ta_2O_5, Fe_2O_3, and TiO_2. Weighed mixtures of

*Corresponding author. Fax: +861062751708.
E-mail address: gbli@chem.pku.edu.cn (G. Li).

0022-4596/$ - see front matter © 2004 Elsevier Inc. All rights reserved.
doi:10.1016/j.jssc.2003.12.025

the four components were homogenized by grinding and preheated at 1200°C for 12 h. They were then grounded, pressed into pellets and heated at 1500°C for 10 h in air followed by a furnace cooling. These were repeated until the equilibrium was reached, which was determined by the X-ray diffraction method. The weights of the samples were monitored before and after heat treatments. The maximum difference was about 2 mg for the total of 6 g of the sample. Therefore, the compositions of the samples were considered to be the same as the initial ones. Sixteen samples were obtained with the nominal formula $BaTi_{1-x}Fe_{x/2}Ta_{x/1}O_3$ ($x = 0.00, 0.02, 0.04, 0.06, 0.08, 0.10, 0.15, 0.20, 0.30, 0.40, 0.50, 0.60, 0.70, 0.90, 0.95, 1.00$), henceforth referred to as BTFT01, BTFT02,…, and BTFT16, respectively.

X-ray diffraction data were collected for all the samples in the system using RINT diffractometer employing Fe$K\alpha$ radiation ($\lambda_{FeK\alpha_1} = 1.93604$, $\lambda_{FeK\alpha_2} = 1.93998$) with an Mn filter operated with 40 kV, 20 mA, under a continuous scanning method with the speed 0.1°/min in the 2θ range of 24°–156°. It was refined with the Rietveld method using the GSAS software package [32,33]. Acceptable fittings (with residual value of $R_p < 4.5\%, R_{wp} < 6.2\%$) were obtained for all samples with the corresponding structure models. The Mössbauer spectrum was obtained using ^{57}Co diffused into rhodium as a source of gamma rays at room temperature [34]. Selected-area diffraction (SAD) and convergent-beam electron diffraction (CBED) were performed on JEM2010FEF under accurate voltage at 100 KV. Bulk specimen was finely crushed in a crucible and dispersed on a supporting grid for transmission electron diffraction (TEM) investigation.

AC impedance data were measured with a HP4192A impedance analyzer with ac voltage of 50 mV and frequency range of 5 Hz to 12 MHz between 25°C and 800°C. The samples were pressed into pellets and sintered again at 1500°C for 20 h and, the density of the samples obtained by Archimedean method was about 90% of their ideal density. Their two faces were then painted with Pt paste and treated at 800°C for 30 min to get a thin Pt film on the surface of the samples.

3. Results and discussion

3.1. Structure analysis

The compositional data and their corresponding lattice parameters are given in Table 1 and illustrated in Figs. 1 and 2. X-ray diffraction indicates that two solid solutions (SS1 and SS2) are to be found in this system while the samples BTFT05 and BTFT06 are two-phase mixtures (Fig. 1). When the unit cell parameters for the samples BTFT01–BTFT06 are plotted against the composition (Fig. 2a), it is clear that

Table 1
Lattice parameters of different phases in the system $BaTi_{1-x}Fe_{x/2}Ta_{x/2}O_3$

Name	x	a_t (Å)[a]	c_t (Å)[a]	a_h (Å)[a]	c_h (Å)[a]
BTFT01	0.00	3.9934(1)	4.0348(1)		
BTFT02	0.02	3.9972(1)	4.0280(1)		
BTFT03	0.04	4.0010(1)	4.0222(1)		
BTFT04	0.06	4.0054(1)	4.0157(1)		
BTFT05	0.08	4.0073(1)	4.0126(1)	5.6719(1)	13.8884(1)
BTFT06	0.10	4.0073(1)	4.0126(1)	5.6719(1)	13.8884(1)
BTFT07	0.15			5.6743(1)	13.8968(1)
BTFT08	0.20			5.6783(1)	13.9072(1)
BTFT09	0.30			5.6863(1)	13.9222(1)
BTFT10	0.40			5.6942(1)	13.9428(1)
BTFT11	0.50			5.7013(1)	13.9660(1)
BTFT12	0.60			5.7092(1)	13.9862(1)
BTFT13	0.70			5.7174(1)	14.0036(1)
BTFT14	0.90			5.7331(1)	14.0464(1)
BTFT15	0.95			5.7371(1)	14.0578(1)
BTFT16	1.00			5.7414(1)	14.0634(1)

[a] a_t and c_t are the lattice parameters a and c of the tetragonal phase, a_h and c_h the lattice parameters a and c of the trigonal phase.

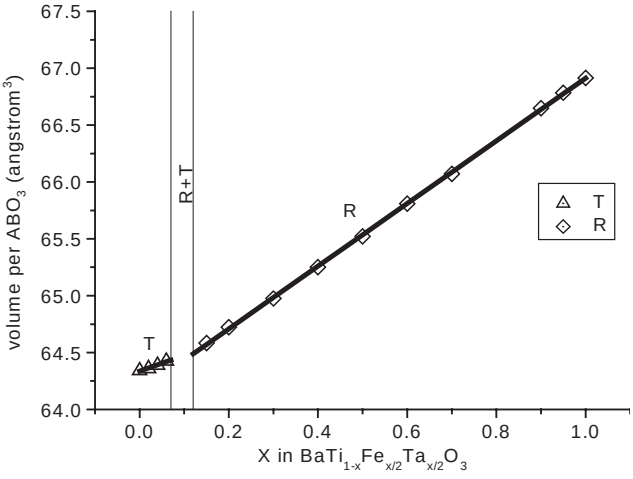

Fig. 1. Comparison of the volume per ABO_3 of the two solid solutions in the series $BaTi_{1-x}Fe_{x/2}Ta_{x/1}O_3$. T, tetragonal solid solution; R, trigonal solid solution.

a linear relationship exists between samples BTFT01–BTFT04 where an increase in Fe/Ta doping of $BaTiO_3$ leads to a decrease in the c-axis and an increase in the a-axis while the remaining two samples are part of a two-phase region. The changes in unit cell parameters with increased doping of Fe/Ta agree well with Vegard's law [35,36] as can be seen in Fig. 2a

$$a_{tx} = a_{t0}(1 - x) + a_{t1}x, \quad (1)$$

$$c_{tx} = c_{t0}(1 - x) + c_{t1}x, \quad (2)$$

where a_{tx}, a_{t0}, a_{t1} and c_{tx}, c_{t0}, c_{t1} are the lattice parameters a and c of the tetragonal $BaTi_{1-x}Fe_{x/2}Ta_{x/2}O_3$, pure tetragonal $BaTiO_3$ and the "supposed tetragonal" $BaFe_{1/2}Ta_{1/2}O_3$; "x" is the composition variable for the

respective sample given in Table 1, $x=(Fe+Ta)/(Ti+Fe+Ta)$.

The samples BTFT07–BTFT15 were all single-phase compounds with the same cell as that of

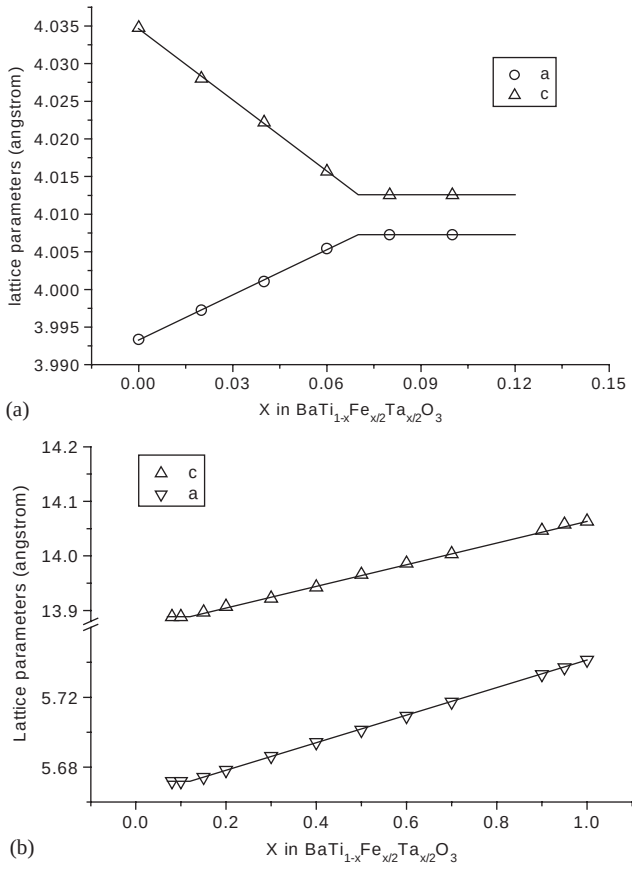

Fig. 2. Variation of the unit cell parameters of the different phases with the average composition ratio "x". "x" is the ratio $(Fe+Ta)/(Ti+Fe+Ta)$ in the sample. (a) tetragonal phase; and (b) trigonal phase.

$Ba(Fe_{1/2}Ta_{1/2})O_3$ (BTFT16). This end member has been reported to have the cubic space group $Pm\bar{3}m$ [37,38]; however, the powder patterns of these samples have been indexed with respect to a trigonal superstructure ($P3m1$) described in a greater detail below. Their lattice parameters a and c are given in Table 1 and the changes in a and c with the composition variable "x" are illustrated in Fig. 2b. The change in the cell parameters agrees well with Vegard's law and can be well expressed as

$$a_{rx} = a_{r0}(1-x) + a_{r1}x, \tag{3}$$

$$c_{rx} = c_{r0}(1-x) + c_{r1}x, \tag{4}$$

where a_{rx}, a_{r0}, a_{r1} and $c_{rx}, c_{r0}, c_{r1}x$, are the lattice parameters a and c of the trigonal $BaTi_{1-x}Fe_{x/2}Ta_{x/2}O_3$, the "supposed trigonal" $BaTiO_3$ and the trigonal end member $Ba(Fe_{1/2}Ta_{1/2})O_3$; "x" is the composition variable as given by $(Fe+Ta)/(Ti+Fe+Ta)$.

The two samples BTFT05 and BTFT06 were found to be of two phases, a tetragonal phase $BaTi_{1-t}Ta_{t/2}Fe_{t/2}O_3$ and a trigonal phase $BaTi_{1-r}Ta_{r/2}Fe_{r/2}O_3$. And using the cell parameters obtained from the GSAS refinement (Table 1) and Eqs. (1)–(4), we obtained a value of 0.07 for "t" and 0.12 for "r" thus giving us the result that the boundaries for $BaTi_{1-x}Fe_{x/2}Ta_{x/2}O_3$ (SS1) exist for values of "x" between 0 and 0.07 while SS2 has the composition range of $0.12 \leqslant x \leqslant 1$.

3.1.1. Solid solution 1 (SS1)

$BaTiO_3$ is tetragonal in the space group $P4mm$ at room temperature [39–41]. The solid solution is formed when small, equimolar amounts of Ta and Fe are substituted for titanium in the structure. A typical X-ray powder diffraction refined using the GSAS program is

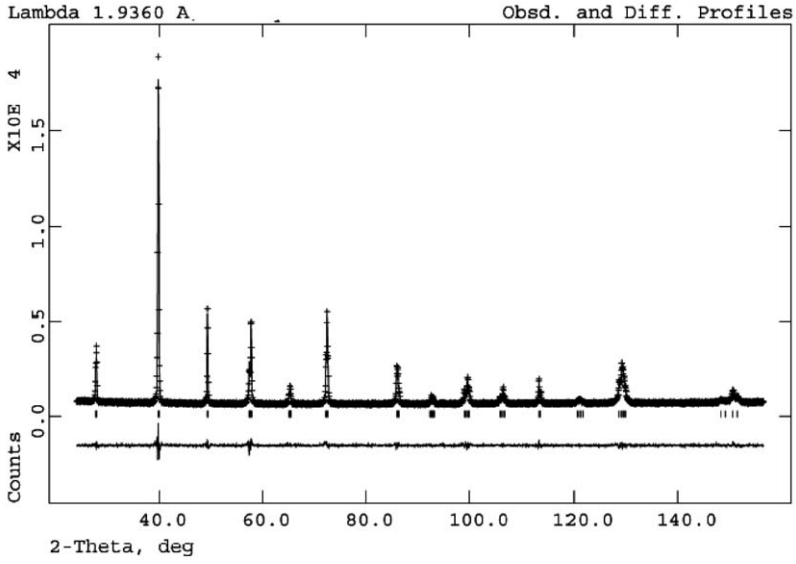

Fig. 3. The Rietveld plot of the powder X-ray diffraction patterns of BTFT03.

Table 2
Rietveld refinement details of BTFT03

Space group	*P4mm*
Lattice parameter (Å)	$a = 4.0010(1)$, $c = 4.0222(1)$
Cell volume (Å^3)	401.473(7)
Ba[a]	0, 0, 0
Ti/Ta/Fe	0.5, 0.5, 0.4916(2)
O1	0.5, 0, 0.5219(3)
O2	0.5, 0.5, 0.0027(3)
R factor	$R_{wp} = 4.6\%$, $R_p = 3.5\%$

[a] The Ba atom has been chosen as the origin.

given in Fig. 3, and the corresponding structural data in Table 2.

3.1.2. Solid solution 2 (SS2)

$Ba(Fe_{1/2}Ta_{1/2})O_3$ (sample BTFT16) is an $A(B'_{1/2}B''_{1/2})O_3$ complex perovskite, where B' and B'' are cations of different valencies; many members of this family with ordered or disordered arrangement of B' and B'' atoms are frequently encountered [42,43]. It has been reported that BTFT16 was cubic [37,38] and the corresponding X-ray diffraction pattern could be very well fitted in the space group $Pm\bar{3}m$ as seen in Table 3

Table 3
Comparison of the different space groups used to describe the structure of BTFT16

Space group	$Pm\bar{3}m$	*R3m*	*P4mm*	*Cm*	*P*1
R factor	$R_p = 4.37\%$, $R_{wp} = 5.99\%$	$R_p = 4.38\%$, $R_{wp} = 5.92\%$	$R_p = 4.37\%$, $R_{wp} = 5.89\%$	$R_p = 4.28\%$, $R_{wp} = 5.66\%$	$R_p = 4.37\%$, $R_{wp} = 5.84\%$
Lattice parameter	$a = 4.0609(1)$ Å	$a = 5.7414(1)$ Å	$a = 4.0611(1)$ Å	$a = 5.7426(1)$ Å	$a = 4.0623(1)$ Å
		$c = 7.0317(1)$ Å	$c = 4.0594(1)$ Å	$b = 5.7418(1)$ Å $c = 4.0590(1)$ Å $\beta = 89.995(1)$	$b = 5.7416(1)$ Å $c = 4.0611(1)$ Å $\alpha = 90.023(1)$ $\beta = 89.993(1)$ $\gamma = 135.012(1)$
Ba	0, 0, 0[a]	0, 0, 0[a]	0, 0, 0[a]	0, 0, 0[a]	0, 0, 0[a]
Ta (Fe)	0.5, 0.5, 0.5	0, 0, 0.5208(1)	0.5, 0.5, 0.5252(1)	0.4831(1), 0, 0.4763(1)	−0.0180(1), 0.4813(1), 0.4744(1)
O1	0.5, 0, 0.5	0.3400(1), 0.1700(1), 0.6876(1)	0.5, 0, 0.4913	0.4762(1), 0, 0.0019(1)	0.0108(1), 0.4737(1), 0.0115(1)
O2			0.5, 0.5, 0.0042(1)	0.2239(1), 0.2474(1), 0.4684(1)	0.4763(1), 0.5081(1), 0.4830(1)
O3					0.5667(1), 0.0171(1), 0.4854(1)

[a] The Ba atom has been chosen as the origin.

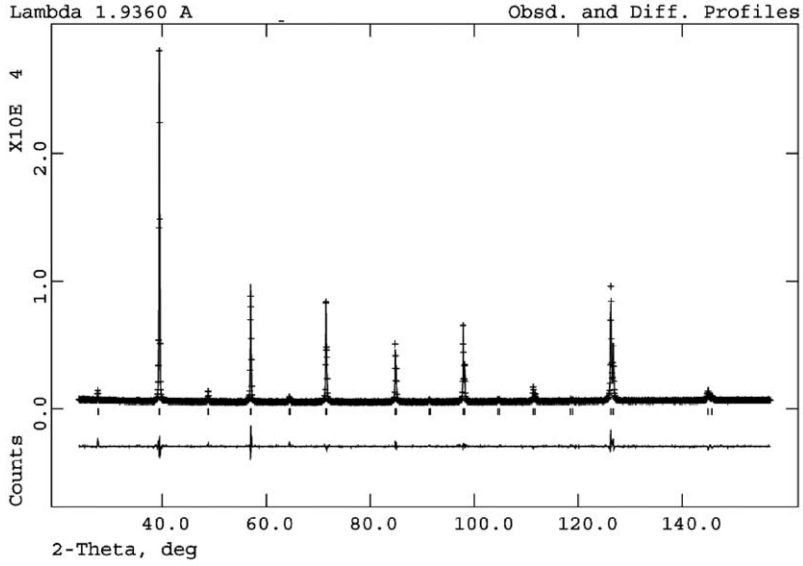

Fig. 4. The Rietveld plot of the powder X-ray diffraction patterns of BTFT16 in the space group $Pm\bar{3}m$.

and Fig. 4. However, the room temperature Mössbauer spectra of this compound shows that it cannot be cubic. As is shown in Fig. 5, a Lorentzian doublet can be fitted to the Mössbauer spectra giving an isomer shift at 0.411 mm s^{-1} and a quadruple splitting of 0.579 mm s^{-1},

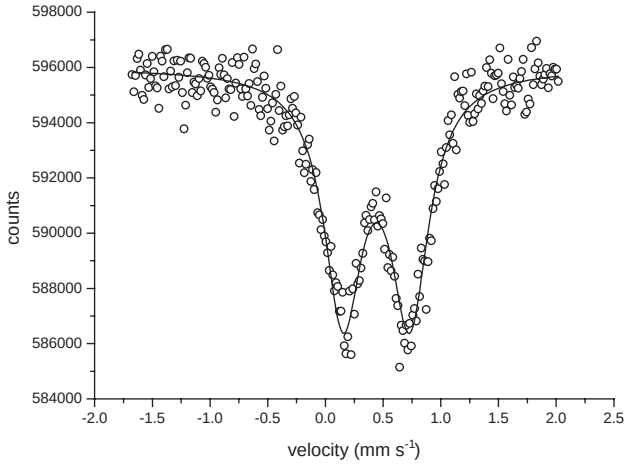

Fig. 5. Mössbauer spectrum of BTFT16 at room temperature obtained using ^{57}Co diffused into rhodium as a source of gamma rays.

indicating that the iron is trivalent in an octahedral coordination. The substantial quadruple splitting observed in the paramagnetic spectra confirmed that the local symmetry at the iron (III) sites cannot be O_h. Therefore, the symmetry of BTFT16 is not cubic. It may however be trigonal, tetragonal, monoclinic or triclinic. For example, four different space groups that agree with the results from the Mössbauer spectra, also fit the diffraction pattern just as well as the cubic $Pm\bar{3}m$ (see Table 3) indicating that powder diffraction alone is not enough to determine the symmetry and the true structure of the compound.

In order to determine the true space group symmetry for BTFT16, a TEM study was also performed using SAD and CBED. Figs. 6a–c shows CBED patterns taken along the $[111]^*$ (a), $[110]^*$ (b) and $[100]^*$ (c) directions of the pseudo-cubic parent.

As seen in Fig. 6a, the symmetry of $3m$ is found in patterns along the $[111]^*$ direction. It is known that this symmetry just appears in a cubic or trigonal cell. As mentioned above, the symmetry of BTFT16 is not cubic. Therefore, the symmetry of BTFT16 is trigonal. The pseudo-cubic cell can been treated as the rhombohedral

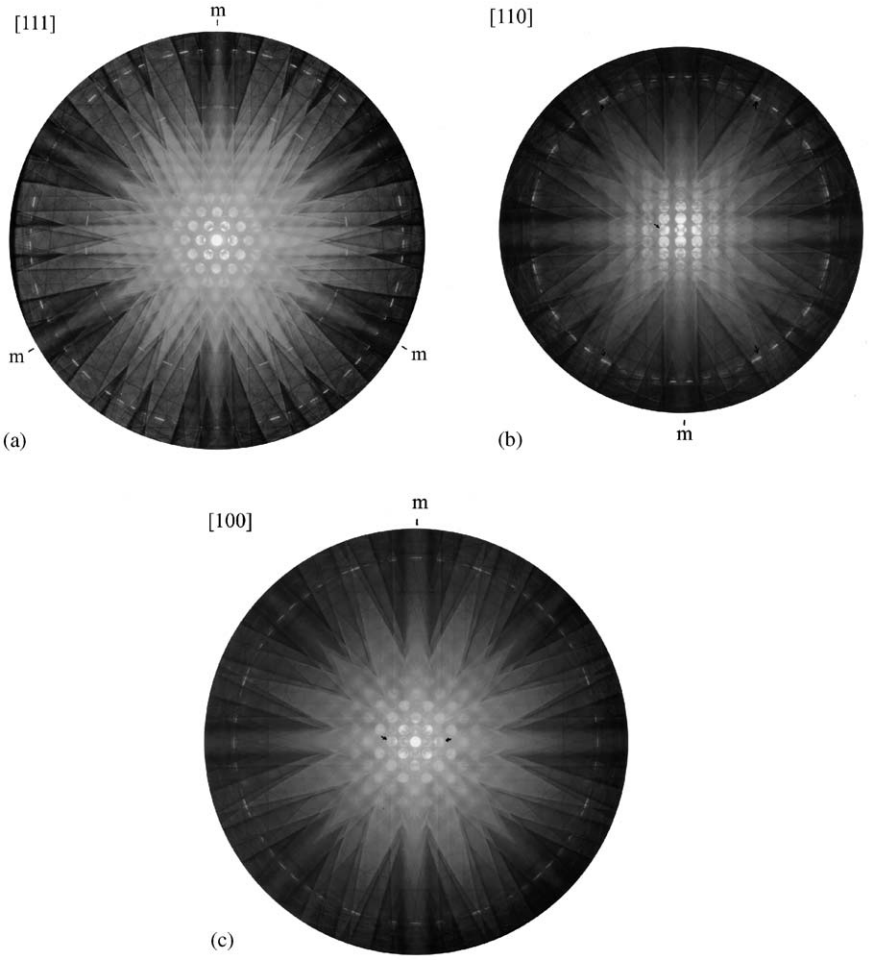

Fig. 6. CBED patterns of BTFT16 along three different directions in the pseudo-cubic symmetry.

cell of the trigonal symmetry, which can be transformed to the hexagonal cell by the following matrix equation:

$$\begin{pmatrix} U \\ V \\ W \end{pmatrix} = \begin{bmatrix} 2/3 & -1/3 & -1/3 \\ 1/3 & 1/3 & -2/3 \\ 1/3 & 1/3 & 1/3 \end{bmatrix} \begin{pmatrix} u \\ v \\ w \end{pmatrix}, \quad (5)$$

$$\begin{pmatrix} H \\ K \\ L \end{pmatrix} = \begin{bmatrix} 1 & 0 & 1 \\ -1 & 1 & 1 \\ 0 & -1 & 1 \end{bmatrix} \begin{pmatrix} h \\ k \\ l \end{pmatrix}, \quad (6)$$

where (U, V, W) is the zone axis index in the hexagonal system; (u, v, w) the zone axis index in the rhombohedral system; (H, K, L) the Miller index in the hexagonal system; and (h, k, l) the Miller index in the rhombohedral system. According to the above matrix, Eq. (5), the $[111]^*$ direction in pseudo-cubic cell is the $[001]^*$ direction in trigonal cell (in hexagonal system). in this case, the possible symmetry for BTFT16 may be $R3m$, $P3m1$ or $P31m$.

In addition, a mirror plane perpendicular to $[-110]^*$ direction is found in patterns along the $[110]^*$ direction in the pseudo-cubic cell (see Fig. 6b). According to the matrix, Eq. (5), this means that a mirror plane perpendicular to $[-100]^*$ direction is found in the patterns along $[122]^*$ direction in the trigonal cell. The space groups $R3m$ and $P3m1$ have such a mirror plane, but $P31m$ does not. Therefore, the possible symmetry for BTFT16 is $R3m$ or $P3m1$. A mirror plane observed in patterns along the $[100]^*$ direction in the pseudo-cubic cell (see Fig. 6c) also agrees with the above suggestion.

Fig. 7 showed the SAD patterns of BTFT16 along different directions with indices in different space groups using the matrix, Eqs. (5) and (6). In the same row, the pattern is the same one indexed in different space groups or unit cell. Weak super-lattice spots were found in the patterns along $[110]^*$ and $[111]^*$ directions in space group $R3m$ with $a = 4.061$ Å and $\alpha = 90°$. They were not indexed in the hexagonal cell transformed from the rhombohedral cell in the same space group $R3m$ with $a = 5.741$ Å, $c = 7.032$ Å and $\alpha = 90°, \gamma = 120°$ (see the second column in Fig. 7). They can be completely indexed in the space group $P3m1$ with $a = 5.741$ Å,

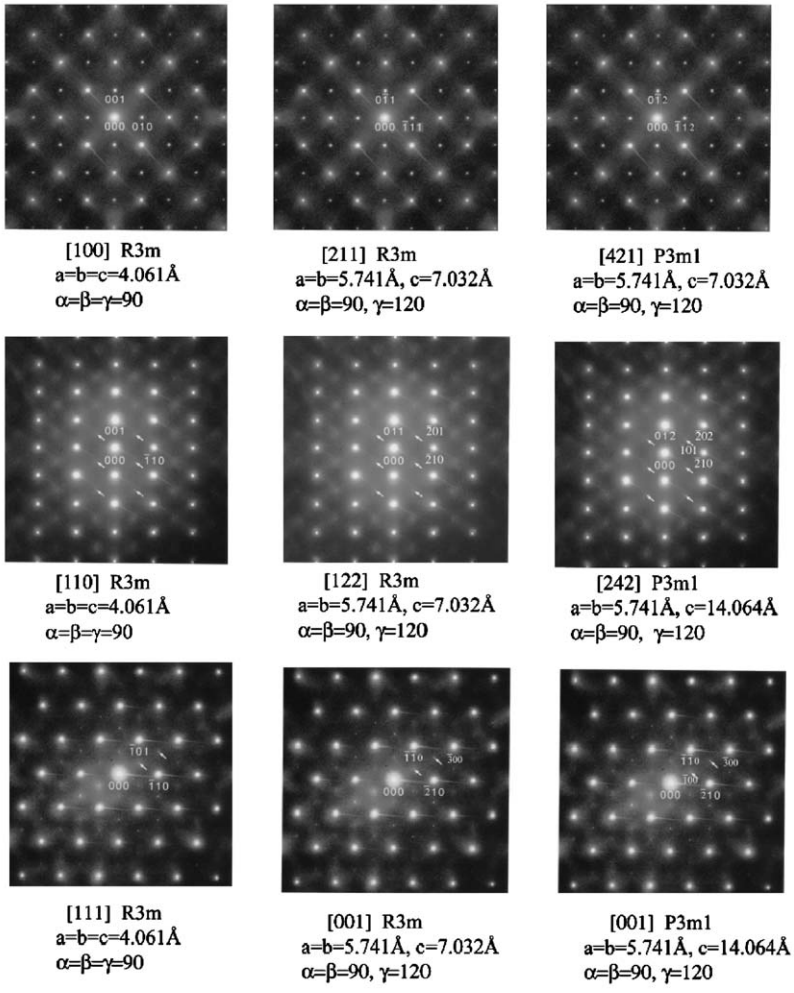

Fig. 7. SAD patterns of BTFT16 along three different directions with interpretations in three different settings of space groups.

$c = 14.064$ Å and $\alpha = 90°, \gamma = 120°$ (see the third column in Fig. 7). These meant that the true symmetry of BTFT16 is $P3m1$ with $a = 5.741$ Å, $c = 14.064$ Å and $\alpha = 90°, \gamma = 120°$.

A final Rietveld refinement of BTFT16 using the super-cell and set in space group $P3m1$ is shown in Fig. 8 and the refinement statistics are given in Table 4. As seen, this fit is as good as those tried previously but this model also fits the data of the TEM and Mössbauer studies.

3.2. Physical properties

3.2.1. Conductivity

The conductivity of the system $BaTi_{1-x}Fe_{x/2}Ta_{x/2}O_3$ has been measured using impedance analyzer HP4192A. The typical impedance spectrum was shown in Fig. 9. It is well known that the impedance spectra of ceramics provide the information of the bulk, grain boundary and electrode [44]. In Fig. 9, the first semicircle is contributed by the bulk and the second semicircle is caused by the grain boundary. The contribution from the grain boundary and electrode are different with different treatments of the samples. Therefore, to give a comparable result, only the bulk conductivity is discussed below.

The conductive behaviors of samples BTFT02–BTFT04 are similar. Their conductivity increases with the increase of the Ta and Fe in $BaTi_{1-x}Fe_{x/2}Ta_{x/2}O_3$ and agreed well with Arrhenius' law as shown in Fig. 10

$$\sigma T = A e^{-E_a/kT}. \quad (7)$$

Here, T is the temperature in Kelvin, σ the conductivity of the samples ($\Omega^{-1}\,cm^{-1}$), E_a the activation energy, and k the Boltzmann's constant. The activation energies 0.81, 0.80 and 0.78 eV for BTFT02, BTFT03 and BTFT04, respectively, are almost identical to 0.80(2) eV and this value is the same as reported by Chan et al. [45] for undoped $BaTiO_3$. A similar mechanism of conductivity, the oxygen vacancy mechanism, is expected.

The conductivity of the samples in SS2 is also very similar and increases with the increase of Fe^{3+} and

Table 4
Rietveld refinement details of BTFT16 in the space group $P3m1$

Space group	$P3m1$
Lattice parameter (Å)	$a = 5.7414(1)$, $c = 14.0634(1)$
Cell volume (Å^3)	401.473(7)
Ba1[a]	0, 0, 0
Ba2	0, 0, 0.4999(1)
Ba3	1/3, 2/3, 0.8331(1)
Ba4	1/3, 2/3, 0.3331(1)
Ba5	2/3, 1/3, 0.6663(1)
Ba6	2/3, 1/3, 0.1663(1)
Ta/Fe1	0, 0, 0.7594(1)
Ta/Fe2	0, 0, 0.2595(1)
Ta/Fe3	1/3, 2/3, 0.5929(1)
Ta/Fe4	1/3, 2/3, 0.0930(1)
Ta/Fe5	2/3, 1/3, 0.9265(1)
Ta/Fe6	2/3, 1/3, 0.4267(1)
O1	0.1633(1), 0.8367(1), 0.6767(1)
O2	0.1633(1), 0.8367(1), 0.1767(1)
O3	0.4967(1), 0.5033(1), 0.0101(1)
O4	0.4967(1), 0.5033(1), 0.5101(1)
O5	0.8300(1), 0.1700(1), 0.8434(1)
O6	0.8200(1), 0.1700(1), 0.3434(1)
R factor	$R_{wp} = 0.061$, $R_p = 0.045$

[a] The Ba1 atom has been chosen as origin.

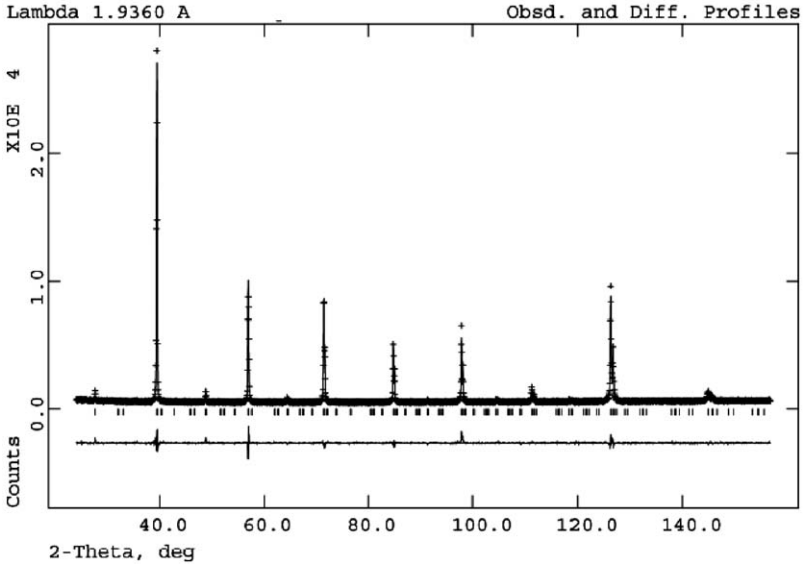

Fig. 8. The Rietveld plot of the powder X-ray diffraction patterns of sample BTFT16 in the space group $P3m1$.

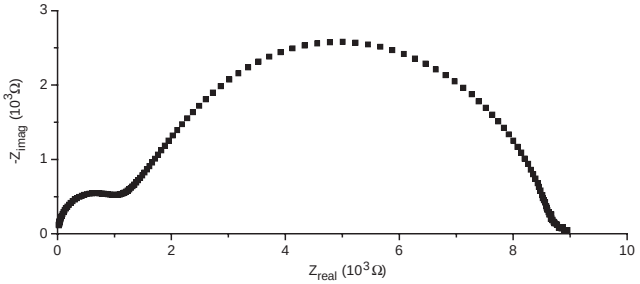

Fig. 9. Impedance spectrum of sample BTFT04 at 460°C.

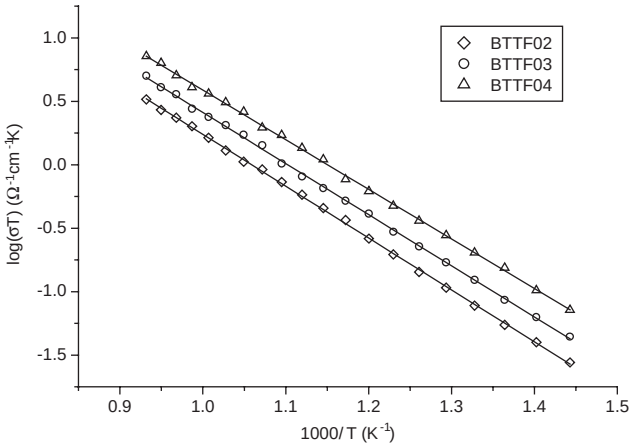

Fig. 10. Temperature dependence of the conductivity for samples BTFT02, BTFT03 and BTFT04.

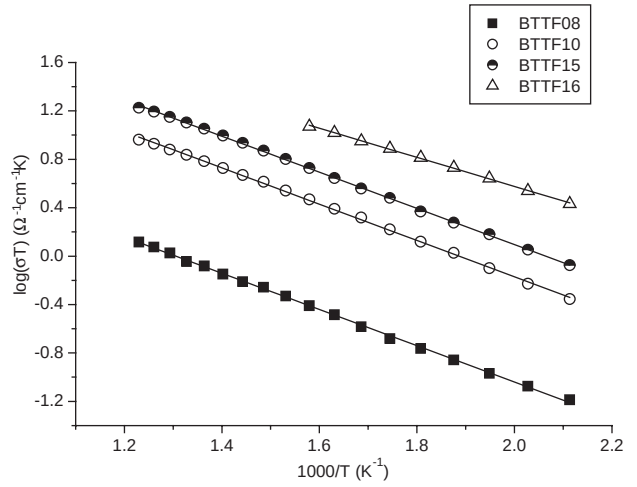

Fig. 11. Temperature dependence of the conductivity for samples BTFT08, BTFT10, BTFT15 and BTFT16.

Ta^{5+} in the samples. Typical temperature-dependent conductivity was shown in Fig. 11 for samples BTFT08, BTFT10 and BTFT15. Their activation energies are all about 0.30 eV. The conductivity of BTFT16 is higher than that of the doped samples with the activation energy of about 0.24 eV, which is the smallest in the whole system $BaTi_{1-x}Fe_{x/2}Ta_{x/2}O_3$. These values are comparable to the reported one for $LaCrO_3$ [46–49]. This indicates that the mechanism of conductivity for

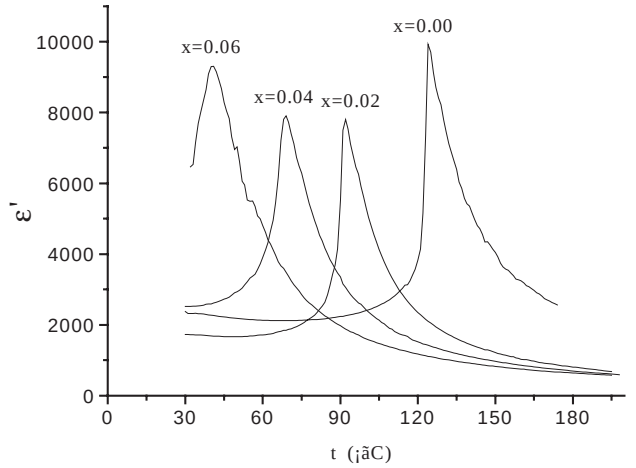

Fig. 12. The temperature dependence dielectric constant at 106 KHz for samples BTFT01–BTFT05. $x = 0.00$, BTFT01; $x = 0.02$, BTFT02; $x = 0.04$, BTFT03; and $x = 0.06$, BTFT04.

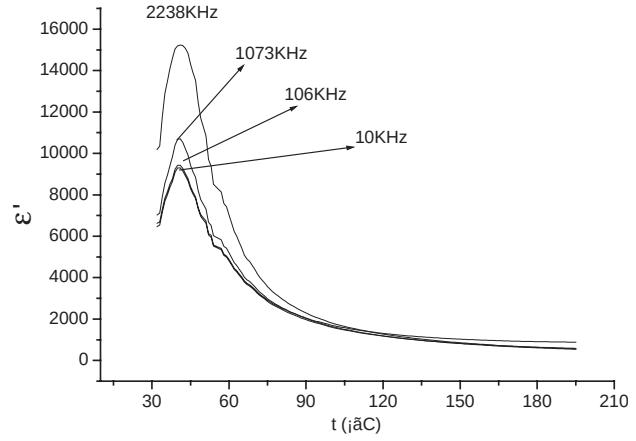

Fig. 13. Frequency dependence dielectric constant of sample BTFT03.

this solution may be similar to that of $LaCrO_3$, which is an electron conductive material.

3.2.2. Dielectric properties

The dielectric properties of samples BTFT01–BTFT04 are very interesting as shown in Fig. 12. The maximum of ε' versus temperature shifts to lower temperature with the decrease of Ti content. It does not change with the frequency although it becomes rounder when the Ti content is less, as shown in Fig. 13. Therefore, the samples in SS1 are classical ferroelectrics.

4. Conclusion

Two solid solutions, tetragonal $BaTi_{1-x}Fe_{x/2}Ta_{x/2}O_3$ ($0 \leqslant x \leqslant 0.07$) and trigonal $BaTi_{1-x}Fe_{x/2}Ta_{x/2}O_3$ ($0.11 \leqslant x \leqslant 1.00$)—SS1 and SS2, respectively, have been found in the system $BaTiO_3$–$BaTa_{1/2}Fe_{1/2}O_3$ at room temperature as shown in Fig. 1. The conductivity of the

compounds in both SS1 and SS2 increases with increasing Fe^{3+} and Ta^{5+} in the solutions. The conductivity in SS2 seems too high to be considered as dielectric materials. The maximum of ε' versus temperature in SS1 shifts towards room temperature when substituting Ti with Fe and Ta. The peak position for the dielectric constant was found not to change with frequency thus no relaxor behavior was found for the compounds in SS1.

Acknowledgments

The authors are thankful for the financial support from NSFC and State Key Basic Research Program of China.

References

[1] B.H. Park, B.S. Kang, S.D. Bu, T.W. Noh, J. Lee, W. Jo, Nature 401 (1999) 682–684.
[2] L.E. Cross, Ferroelectrics 151 (1994) 305.
[3] N. Setter, L.E. Cross, J. Appl. Phys. 51 (1980) 4356.
[4] H. Ardnt, F. Sauerbier, G. Schmidt, A. Shebanov, Ferroelectrics 79 (1988) 145.
[5] G.A. Smolenski, V.A. Isupov, Dokl. Akad. Nauk. SSSR 9 (1954) 653.
[6] G.A. Smolenskii, V.A. Isupov, A.I. Agranovskaya, S.N. Popov, Sov. Phys. Solid State 2 (1961) 2584.
[7] R.M. Glaister, J. Am. Ceram. Soc. 43 (1960) 348.
[8] P. Gallagher, J. Am. Ceram. Soc. 46 (1963) 359.
[9] A.I. Kashilinski, V.I. Chechernikov, Yu.N. Venevtsev, Sov. Phys. Solid State 8 (1967) 2074.
[10] I.H. Ismailzade, R.M. Ismailov, Phys. Stat. Sol. (a) 59 (1980) K191.
[11] M. Mahesh Kumar, M.B. Suresh, S.V. Suryanarayana, G.S. Kumar, J. Appl. Phys. 6811 (1998) 84.
[12] M. Mahesh Kumar, M.B. Suresh, S.V. Suryanarayana, J. Appl. Phys. 86 (1999) 1634.
[13] Chen Ang, Zhi Yu, Zhi Jing, Phys. Rev. B 61 (2000) 957.
[14] T. Mitsui, W.B. Westphal, Phys. Rev. 124 (1961) 1354.
[15] J.G. Bednorz, K.A. Muller, Phys. Rev. Lett. 52 (1984) 2289.
[16] G.I. Skanavi, I.M. Ksendzov, V.A. Trigubenko, V.G. Prokhvatilov, Sov. Phys. JETP 6 (1958) 250.
[17] Chen Ang, Zhi Yu, P.M. Vilarinho, J.L. Baptista, Phys. Rev. B 57 (1998) 7403.
[18] G.A. Smolenskii, V.A. Isupov, V.I. Agranovskaya, S.V. Popov, Sov. Phys. Solid State 2 (1967) 2584.
[19] A.N. Gubkin, A.M. Kashtanova, G.I. Skanavi, Sov. Phys. Solid State 3 (1961) 807.
[20] Chen Ang, Zhi Yu, J. Hemberger, P. Lukenheimer, A. Loidl, Phys. Rev. B. 59 (1999) 6665.
[21] Chen Ang, Zhi Yu, J. Hemberger, P. Lukenheimer, A. Loidl, Phys. Rev. B. 59 (1999) 6670.
[22] R.K. Dwivedi, D. Kumar, O. Parkash, J. Phys. D 33 (2000) 88.
[23] O. Parkash, L. Pandey, M.K. Sharma, D. Kumar, J. Mater. Sci. 24 (1989) 4505.
[24] U.T. Hochli, K. Knorr, A. Loidl, Adv. Phys. 39 (1990) 405.
[25] B.E. Vugmeister, M.D. Glinchuk, Rev. Mod. Phys. 62 (1990) 993.
[26] J. Toulouse, B.E. Vugmeister, R. Pattnaik, Phys. Rev. Lett. 73 (1994) 3467.
[27] P. Doussineau, C. Frenois, A. Levelut, J. Toulouse, S. Ziolkiewicz, Ferroelectrics 150 (1993) 59.
[28] P. Doussineau, Y. Farssi, C. Frenois, A. Levelut, K. McEnaney, J. Toulouse, S. Ziolkiewicz, Europhys. Lett. 24 (1993) 415.
[29] H.-M. Christen, U.T. Hochli, A. Chatelain, S. Ziolkiewicz, J. Phys.: Condens. Matter 3 (1991) 8387.
[30] M. Fukushima, G.B. Li, Y. Uesu, K. Kohn, Ferroelectrics 286 (2003) 801–806.
[31] G.B. Li, Y. Uesu, K. Kohn, J. Solid State Chem. 164 (2002) 98–105.
[32] A.C. Larson, R.B. von Dreele, Report LAUR 86–748, Los Alamos National Laboratory, 1985.
[33] H.M. Rietveld, J. Appl. Crystallogr. 2 (1969) 65–71.
[34] R.L. Mössbauer, Z. Phys. 151 (1958) 124.
[35] L. Vegard, Z. Phys. 5 (1921) 17.
[36] L. Vegard, Z. Kristallogr. 67 (1928) 239.
[37] A.I. Agranovskaya, Izves. Akad. Nauk. SSSR, Ser. Fiz. 24 (1960) 1275–1281.
[38] V.S. Filip'ev, E.G. Fesenko, Kristallogrfiya 6 (1961) 770–772.
[39] H.H. Weider, Phys. Rev. 99 (1955) 1161.
[40] W. Merz, Phys. Rev. 76 (1949) 1221.
[41] J. Roth, M. Uhrmacher, P. de la Presa, L. Ziegeler, K.P. Lieb, Z. Naturforsch. 55 (2000) 242.
[42] E.D. Fesensko, Perovskite Family and Ferroelectricity, Atomisdat, Moscow, 1971 (in Russian).
[43] F.S. Galasso, Structure, Properties and Preparation of Perovskite-type Compounds, Pergamon Press, Oxford, 1969.
[44] J.C.C. Abrantes, J.A. Labrincha, J.R. Frade, Mater. Res. Bull. 35 (2000) 955–964.
[45] N.-H. Chan, R.K. Sharma, D.M. Smyth, J. Am. Ceram. Soc. 64 (1981) 556–562.
[46] G.B. Li, X.J. Kuang, Sh.J. Tian, F.H. Liao, X.P. Jing, Y. Uesu, K. Kohn, J. Solid State Chem. 165 (2002) 381–392.
[47] D.P. Karim, A.T. Aldred, Phys. Rev. B 20 (1979) 2255–2263.
[48] K. Azegami, M. Yoshinaka, K. Hirota, O. Yamaguchi, Mater. Res. Bull. 33 (1998) 341–348.
[49] M. Panneerselvam, K.J. Rao, J. Mater. Chem. 13 (2003) 596–601.